

1 **Persistence of SARS CoV-2 S1 Protein in CD16+ Monocytes**
2 **in Post-Acute Sequelae of COVID-19 (PASC) Up to 15 Months**
3 **Post-Infection**

4 Summary: SARS CoV-2 S1 protein in CD16+ monocytes in the absence of full-length
5 RNA in patients with PASC up to 15 months post-infection

6 Bruce K. Patterson¹, Edgar B. Francisco¹, Ram Yogendra², Emily Long¹, Amruta Pise¹, Hallison
7 Rodrigues¹, Eric Hall³, Monica Herrera³, Purvi Parikh⁴, Jose Guevara-Coto^{5,6}, Timothy J.
8 Triche⁷, Paul Scott⁷, Saboor Hekmati⁷, Dennis Maglinte⁷, Xaiolan Chang⁸, Rodrigo A Mora-
9 Rodríguez⁵, Javier Mora⁵

10

11

12 ¹IncellDx Inc, San Carlos, CA

13 ²Lawrence General Hospital, Lawrence, MA

14 ³Bio-Rad Laboratories, Hercules, CA

15 ⁴NYU Langone Health, New York, NY

16 ⁵Lab of Tumor Chemosensitivity, CIET / DC Lab, Faculty of Microbiology, Universidad
17 de Costa Rica

18 ⁶Department of Computer Science and Informatics (ECCI), Universidad de Costa Rica,
19 San Jose, Costa Rica

20 ⁷Avrok Laboratories, Inc., Azusa, CA

21 ⁸ Vaccine & Gene Therapy Institute and Oregon National Primate Research Center,
22 Oregon Health & Science University, Portland, OR, USA

23

24

25 Summary: SARS CoV-2 S1 Protein in CD16+ Monocytes In PASC

26

27

28 Corresponding author:

29 Bruce K. Patterson MD

30 1541 Industrial Road

31 San Carlos, CA 94070

32 Tel: +1.650.777.7630

33 Fax: +1.650.587.1528

34 Email: brucep@incelldx.com

35

36 **Key words:**

37

38 COVID-19, PASC, SARS CoV-2 S1 protein, non-classical monocytes, CCR5, fractalkine

39

40

41

42

43

44
45
46
47
48
49
50
51
52
53
54
55
56
57
58
59
60
61
62
63
64
65
66
67
68
69
70
71
72
73
74
75
76
77
78
79
80
81
82
83
84
85
86
87

ABSTRACT

The recent COVID-19 pandemic is a treatment challenge in the acute infection stage but the recognition of chronic COVID-19 symptoms termed post-acute sequelae SARS-CoV-2 infection (PASC) may affect up to 30% of all infected individuals. The underlying mechanism and source of this distinct immunologic condition three months or more after initial infection remains elusive. Here, we investigated the presence of SARS-CoV-2 S1 protein in 46 individuals. We analyzed T-cell, B-cell, and monocytic subsets in both severe COVID-19 patients and in patients with post-acute sequelae of COVID-19 (PASC). The levels of both intermediate (CD14+, CD16+) and non-classical monocyte (CD14Lo, CD16+) were significantly elevated in PASC patients up to 15 months post-acute infection compared to healthy controls ($P=0.002$ and $P=0.01$, respectively). A statistically significant number of non-classical monocytes contained SARS-CoV-2 S1 protein in both severe ($P=0.004$) and PASC patients ($P=0.02$) out to 15 months post-infection. Non-classical monocytes were sorted from PASC patients using flow cytometric sorting and the SARS-CoV-2 S1 protein was confirmed by mass spectrometry. Cells from 4 out of 11 severe COVID-19 patients and 1 out of 26 PASC patients contained ddPCR+ peripheral blood mononuclear cells, however, only fragmented SARS-CoV-2 RNA was found in PASC patients. No full length sequences were identified, and no sequences that could account for the observed S1 protein were identified in any patient. Non-classical monocytes are capable of causing inflammation throughout the body in response to fractalkine/CX3CL1 and RANTES/CCR5.

88

89 INTRODUCTION

90

91 Post-acute sequelae SARS-CoV-2 infection (PASC) is a disabling and sometimes debilitating
92 condition that occurs in 10%-30% of individuals infected by SARS-CoV-2 and has recently been
93 proposed to cause neurologic symptoms in 30% of those infected (1). The number and extent of
94 symptoms is extremely heterogeneous with some reports suggesting >200 different symptoms
95 (2). The underlying cause of PASC symptoms has remained a mystery though some data has
96 pointed to tissue reservoirs of persistent SARS-CoV-2 as a potential mechanism (3,4). We
97 recently reported a machine learning approach that identified the unique immunologic signature
98 of individuals with PASC (5). In the same report, we also identified characteristic immune cell
99 subset abnormalities that accompanied the unique cytokine/chemokine profile. The predominant
100 immune cell abnormality was elevations in monocyte subsets. Monocyte subpopulations are
101 divided into 3 phenotypic and functionally distinct types. Classical monocytes exhibit the
102 CD14⁺⁺, CD16⁻ phenotype, intermediate monocytes exhibit a CD14⁺, CD16⁺ phenotype, and
103 the non-classical monocytes express CD14^{lo}, CD16⁺ (6,7). Further they express very different
104 cell surface markers as previously described. In particular, classical monocytes express high
105 levels of the ACE-2 receptor, the putative receptor for SARS-CoV-2 (8). Intermediate and non-
106 classical monocytes express very little ACE-2 receptor. Similarly, classical monocytes express
107 low levels of the chemokine receptors CX3R1 and CCR5. Intermediate monocytes express high
108 levels of CCR5 while non-classical monocytes express high levels of CX3R1. Here, we report
109 kinetic differences in the proportions of monocyte subsets in severe cases and PASC, as well as
110 the presence of SARS-CoV-2 protein unaccompanied by corresponding viral RNA in CD14^{lo},
111 CD16⁺ monocytes in PASC patients up to 16 months post-acute SARS-CoV-2 infection.

112

113 **RESULTS**

114 Similar to other inflammatory and infectious conditions such as sepsis, lupus erythematosus, and
115 rheumatoid arthritis among others (9), we detected statistically significant increases ($P < 0.002$) of
116 intermediate CD14⁺, CD16⁺ monocytes in individuals with PASC compared to healthy controls.
117 In addition, CD14^{lo}, CD16⁺ non-classical monocytes were also significantly elevated in PASC
118 ($P = 0.01$). Neither intermediate nor non-classical monocytes were elevated in severe COVID-19
119 (Figure 1).

120

121 Since the reports by our group and others found that monocyte subsets can be infected by HIV,
122 HCV, Zika virus and Dengue fever virus (10-12), we screened peripheral blood mononuclear
123 cells (PBMCs) from PASC individuals, as well as acute severe COVID-19 as controls, for
124 SARS-CoV-2 RNA (Table 1). Using the highly sensitive, quantitative digital droplet PCR
125 (ddPCR), we found that 36% (4 of 11) of severe COVID-19 patients' PBMCs contained SARS-
126 CoV-2 RNA compared to 4% (1/26) of PASC patients' PBMCs. The one PASC patient that was
127 RNA positive was 15 months post infection.

128

129 To further establish the exact reservoir contributing to the positive signal detected using ddPCR,
130 we performed high parameter flow cytometry with antibodies that define B cell, T-cell, and
131 monocytic subsets in addition to simultaneous staining of these cells with an antibody for the
132 SARS-CoV-2 S1 protein. As demonstrated in Figure 2, we found distinct subpopulations of
133 SARS-CoV-2 containing cells in the CD14^{lo}, CD16⁺ monocytic subset for 73% (19 out of 26)
134 of PASC patients and 91% (10 out of 11) of severe COVID-19 patients. As demonstrated in
135 Figure 3, the quantity of SARS-CoV-2 S1 containing cells were statistically significant in both

136 the severe patients (P=0.004) and in the PASC patients (P=0.02). Neither classical monocytes
137 nor intermediate monocytes expressed the SARS-CoV-2 S1 protein.

138

139 To confirm the presence of SARS-CoV-2 S1 protein, we sorted CD14^{lo}, CD16⁺ monocytes and
140 performed Ultra High-Performance Liquid Chromatography (UHPLC). Following
141 immunoprecipitation, the elution fractions were dried down *in vacuo*, resuspended in ddH₂O and
142 purified by to remove any non-crosslinked SARS-CoV-2 S1 antibody as well as any detergents
143 from the commercial immunoprecipitation buffers. The UHPLC collected fractions were dried *in*
144 *vacuo*, resuspended in 100 mM HEPES (pH 8.0, 20% Acetonitrile), and subjected to cistern:
145 reduction and alkylation with chloroacetamide. The samples were then digested with AspN and
146 LysC endopeptidases for 16h at 37°C. The digested peptides were analyzed on an Agilent 6550
147 IonFunnel QTOF and 1290 UHPLC by comparing patient samples to identical digests performed
148 on commercially available SARS-CoV-2 S1 subunit. S1 subunit peptides from patient samples
149 were mapped to a peptide database generated using commercial S1 subunit digests. Peptide
150 identification consisted of matches in exact mass, isotope distribution, peptide charge state, and
151 UHPLC retention time. As shown in Figure 4, the retention time of the representative peptide
152 NLREFVFK in the digested commercial S1 subunit and Sample LH1-6 matched. Additionally,
153 the Mass Spectra in Figure 4 show identical mass, isotope distribution, and charge states for the
154 representative peptide NLREFVFK in the representative LH1 sample and commercial S1 subunit
155 (also observed in LH 2-6, not shown). Using these metrics, up to 44% of the S1 subunit peptides
156 could be identified in patient samples LH1-LH6 (Supplementary Table 1), providing
157 complementary evidence to flow cytometry experiments that demonstrate the presence of S1
158 subunit protein in these patient cells.

159 To determine whether the observed S1 spike protein was a product of persistent viral infection,
160 whole viral genome sequencing was performed on monocytes from five patients. Coverage
161 analysis of the human control amplicons revealed adequate coverage to positively identify
162 human genomic content. This is consistent with extraction of viral genomic content from a
163 human host. Human controls also included targeted amplicons for amelogenin (*AMELX* and
164 *AMELY*). The ratio of *AMELX* and *AMELY* reads is consistent with the known genders of each
165 sample.

166 The sequencing coverage for the five samples was consistent with low viral titer samples or
167 samples with high Ct values. Average coverage was between 24.17-592.87x and percent bases
168 covered at 10x and 20x was between 10.81-19.18% and 7.69-15.24% respectively (Table 2).
169 This is well below the expected threshold to eliminate stretches of Ns > 99 for consensus
170 sequence submission to GenBank and > 90% genome coverage at 10x for accurate lineage
171 determination and sequence submission to GISAID (www.gisaid.org). Evaluation of the reads
172 revealed predominantly short reads (<100bp). To address poor quality reads, primer-dimers or
173 reads that could possibly map to multiple loci, reads < MAPQ 10 were filtered resulting in the
174 removal of 3.63-18.99% of total reads per sample.

175 Lineage determination of the five samples from high quality mutations in the callable regions
176 yielded lineages of *B* and *B.1* and were non-specific due to inadequate coverage across the
177 genome. Mutations were identified in *ORF1ab* in all but sample LH5. LH5 had mutations in *N*,
178 *S*, and *ORF3b*. (Figure 5).

179

180 **DISCUSSION**

181 Here, we report the discovery of persistent SARS-CoV-2 protein in CD14^{lo}, CD16⁺ monocytes
182 out to 15 months in some individuals and discuss the implications for the pathogenesis of PASC
183 and severe cases of COVID-19. The three subtypes of circulating monocytes (classical,
184 intermediate, non-classical) express very different cell surface molecules and serve very different
185 functions in the immune system. Generally, classical' monocytes exhibit phagocytic activity,
186 produce higher levels of ROS and secrete proinflammatory molecules such as IL-6, IL-8, CCL2,
187 CCL3 and CCL5. Intermediate monocytes express the highest levels of CCR5 and are
188 characterized by their antigen presentation capabilities, as well as the secretion of TNF- α , IL-1 β ,
189 IL-6, and CCL3 upon TLR stimulations. Non-classical monocytes expressing high levels of
190 CX3CR1 are involved in complement and Fc gamma-mediated phagocytosis and anti-viral
191 responses (6).

192 After maturation, human monocytes are released from bone marrow into the circulation as
193 classical monocytes. Currently, strong evidence supports the concept that intermediate and non-
194 classical monocytes emerge sequentially from the pool of classical monocytes (13). This is
195 supported by transcriptome analysis showing that CD16⁺ monocytes have a more mature
196 phenotype (14). In humans, 85% of the circulating monocyte pool are classical monocytes,
197 whereas the remaining 15% consist of intermediate and nonclassical monocytes (13). Classical
198 monocytes have a circulating lifespan of approximately one day before they either migrate into
199 tissues, die, or turn into intermediate and subsequently nonclassical monocytes (6,13).

200 During pathologic conditions mediated by infectious/inflammatory reactions, the proportions of
201 monocyte subsets vary according to the functionality of each specific subpopulation (6,13,15).

202 Our previous results show that during early stages of the disease, PASC group have reduced
203 classical monocyte and increased intermediate monocyte percentages compared with healthy

204 controls (5). We find an increase in nonclassical monocytes in PASC group 6-15 months post
205 infection, and higher percentages of intermediate and nonclassical monocytes at day 0 in severe
206 cases, suggesting augmented classical-intermediate-nonclassical monocyte transition in both
207 groups but with different kinetics.

208 The clinical relevance of monocyte activation in COVID-19 patients and the significance of
209 these cells as viral protein reservoir in PASC is supported by our data reporting the presence of
210 S1 protein within nonclassical monocytes. Viral particles and/or viral proteins can enter
211 monocyte subpopulations in distinct ways, and this appears to be regulated differently in
212 individuals that will develop severe disease or PASC. Classical monocytes are primarily
213 phagocytes and express high levels of the ACE-2 receptor (8). Therefore, they could either
214 phagocyte viral particles and apoptotic virally infected cells or be potential targets for SARS-
215 CoV-2 infection. Considering their short circulating lifespan, viral protein-containing classic
216 monocytes turn into intermediate and nonclassical monocytes. According to our results, this
217 process happens faster in the severe group than in the PASC group. Indeed, at early stages of the
218 disease the severe group show increased nonclassical monocytes whereas in PASC both the
219 intermediate monocytes and non-classical monocytes are elevated. Additionally, CD14⁺CD16⁺
220 monocytes express intermediate levels of ACE-2 receptors and could as well serve as an
221 infectious target of SARS-CoV-2 as it has been proved to be an infectious target of HIV-1 and
222 HCV¹¹. Nonclassical monocytes have been proposed to act as custodians of vasculature by
223 patrolling endothelial cell integrity (16), thus pre-existing CD14^{lo} CD16⁺ cells could ingest
224 virally infected apoptotic endothelial cells augmenting the proportion of nonclassical monocytes
225 containing S1 protein. This mechanism is more likely to take place in the PASC group where the
226 S1 protein was detected 12-15 months post infection than in the severe group. Furthermore,

227 nonclassical monocytes are associated with FcR-mediated phagocytosis (17,18), which might be
228 related with the ingestion of opsonized viral particles after antibody production at later stages of
229 the disease in PASC.

230 Previous reports indicate that the numbers of classical monocytes decrease, but the numbers of
231 intermediate and non-classical monocytes increase in COVID-19 patients (19). Thus, the
232 presence of S1 protein in nonclassical monocytes in both severe and PASC, might be associated
233 with clinical characteristics and outcome of these groups. Previously, we found that individuals
234 with severe COVID-19 have high systemic levels of IL-6, IL-10, VEGF and sCD40L (5).

235 Consistent with our data, other studies showed association of increased production of IL-6,
236 VEGF and IL-10 by nonclassical monocytes with disease severity (20-22).

237 In the case of PASC, the persistence of circulating S1-containing nonclassical monocytes up to
238 16 months post infection, independently of the different possible mechanisms of viral proteins
239 internalization discussed above, indicates that certain conditions are required to maintain this cell
240 population. It has been shown in both humans and mice that nonclassical monocytes require
241 fractalkine (CX3CL1) and TNF to inhibit apoptosis and promote cell survival (22). Our previous
242 data show high IFN- γ levels in PASC individuals (5), which can induce TNF- α production (23).
243 Further, TNF- α and IFN- γ induce CX3CL1/Fractalkine production by vascular endothelial cells²⁴
244 creating the conditions to promote survival of nonclassical monocytes. Another important aspect
245 is the permanency of S1-containing cells in the circulation, intermediate monocytes express high
246 levels of CCR5 and extravasation of these cells can occur in response to CCL4 gradients. We
247 showed that PASC individuals have low levels of CCL4 (5) maintaining these cells in circulation
248 until they turn into nonclassical monocytes. Moreover, IFN- γ induced CX3CL1/Fractalkine

249 production by endothelial cells (23) creates a gradient within the vascular compartment
250 preserving nonclassical monocytes expressing CX3CR1 in the circulation.

251 Nonclassical monocytes are usually referred as anti-inflammatory cells (22), nevertheless it was
252 recently shown that this subset can acquire a proinflammatory phenotype (25). Nonclassical
253 monocytes acquire hallmarks of cellular senescence, which promote long term survival of these
254 cells in circulation as explained above. Additionally, this induces an inflammatory state of the
255 non-classical monocytes that could be a manifestation of the senescence-associated secretory
256 phenotype (SASP), characterized by a high basal NF- κ B activity and production of pro-
257 inflammatory cytokines such as IL-1 α , TNF- α and IL-8 (25).

258 The hallmark of PASC is the heterogeneity of symptoms arising in a variety of tissues and
259 organs. These symptoms are likely associated with the inflammatory phenotype of these
260 senescent nonclassical monocytes. The CD14^{lo}, CD16⁺, S1 protein⁺ monocytes could be
261 preferentially recruited into anatomic sites expressing fractalkine and contribute to vascular and
262 tissue injury during pathological conditions in which this monocyte subset is expanded as
263 previously demonstrated in non-classical monocytes without S1 protein. Previously, CD16⁺
264 monocytes were demonstrated to migrate into the brain of AIDS patients expressing high levels
265 of CX3CL1 (fractalkine) and SDF-1 (26), and mediate blood-brain barrier damage and neuronal
266 injury in HIV-associated dementia via their release of proinflammatory cytokines and neurotoxic
267 factors. These sequelae are very common in PASC and these data could represent the underlying
268 mechanism for the symptoms. Interestingly, a number of papers have been written discussing the
269 increased mobilization of CD14^{lo}, CD16⁺ monocytes with exercise (27). These data support the
270 reports of worsening PASC symptoms in individuals resuming pre-COVID exercise regimens. In
271 summary, the mechanism of PASC discussed in this report suggests that intermediate monocytes

272 remain in circulation due to low CCL4 levels extending their time to differentiate leading to an
273 accumulation of non-classical monocytes. The utility of using CCR5 antagonists in preventing
274 migration of intermediate and non-classical monocytes due to the elevated levels of
275 CCL5/RANTES in PASC (5). Further, our data suggests that interruption of the
276 CX3CR1/fractalkine pathway would be a potential therapeutic target to reduce the survival of
277 S1-containing non-classical monocytes and the associated vascular inflammation previously
278 discussed (5) and presented here.

279 It is important to note that the S1 protein detected in these patients appears to be retained from
280 prior infection or phagocytosis of infected cells undergoing apoptosis and is not the result of
281 persistent viral replication. Full length sequencing of the five cases submitted for genomic
282 analysis failed to identify any full-length sequence in the spike protein gene, or any other gene,
283 that could account for the observed spike protein detected by proteomic analysis. In contrast,
284 fragmented SARS-CoV-2 sequence was identified in all five of the cases. We have observed a
285 pattern of high Ct value or negativity by PCR, accompanied by scant, fragmented viral sequence
286 identified by whole viral genome sequencing over the past several months, a major shift from the
287 low Ct value, full length viral sequences identified throughout most of 2020. The reasons for this
288 shift are unclear, but as seen in these cases, it is unlikely these patients are producing any
289 replication competent viral genomes, and are thus incapable of transmitting the infection. In
290 contrast, the patients reported here appear to have developed an immune response to retained
291 viral antigens, specifically the S1 fragment of the spike protein, which continues to be presented
292 by CD16+ monocytes, eliciting an innate immune response characterized by elevated
293 inflammatory markers including interferon γ , IL-6, IL-10, and IL-2, among others. The body of
294 evidence reported here would not support continued viral replication. Instead, it implicates

295 dysregulation of innate immunity inflammatory mediators in response to persistent viral protein
296 presentation by CD16+ monocytes.

297

298 **MATERIAL/METHODS**

299 *Patients*

300 Following informed consent, whole blood was collected in a 10 mL EDTA tube and a 10 mL plasma
301 preparation tube (PPT). A total of 144 individuals were enrolled in the study consisting of 29 normal
302 individuals, 26 mild-moderate COVID-19 patients, 25 severe COVID-19 patients and 64 chronic COVID
303 (long hauler-LH) individuals. Long Haulers symptoms are listed in Figure 1. Study subjects were
304 stratified according to the following criteria.

305 Mild

- 306 1. Fever, cough, sore throat, malaise, headache, myalgia, nausea, diarrhea, loss of taste and smell
- 307 2. No sign of pneumonia on chest imaging (CXR or CT Chest)
- 308 3. No shortness of breath or dyspnea

309 Moderate:

- 310 1. Radiological findings of pneumonia fever and respiratory symptoms
- 311 2. Saturation of oxygen (SpO₂) ≥ 94% on room air at sea level

312 Severe

- 313 1. Saturation of oxygen (SpO₂) < 94% on room air at sea level
- 314 2. Arterial partial pressure of oxygen (PaO₂)/ fraction of inspired oxygen (FiO₂) < 300mmHG
- 315 3. Lung infiltrate > 50% within 24 to 48 hours
- 316 4. HR ≥ 125 bpm
- 317 5. Respiratory rate ≥ 30 breaths per minute

318 Critical

- 319 1. Respiratory failure and requiring mechanical ventilation, ECMO, high-flow nasal cannula oxygen
320 supplementation, noninvasive positive pressure ventilation (BiPAP, CPAP)
321 2. Septic Shock- Systolic blood pressure < 90mmHg or Diastolic blood pressure < 60 mmHg or
322 requiring vasopressors (levophed, vasopressin, epinephrine)
323 3. Multiple organ dysfunction (cardiac, hepatic, renal, CNS, thrombotic disease)

324

325 Post-acute COVID-19 (Long COVID)

- 326 1. Extending beyond 3 weeks from the initial onset of first symptoms

327 Chronic COVID-19

- 328 1. Extending beyond 12 weeks from the initial onset of first symptoms (Table 1S)

329

330 *High Parameter Immune Profiling/Flow Cytometry*

331 Peripheral blood mononuclear cells were isolated from peripheral blood using Lymphoprep density
332 gradient (STEMCELL Technologies, Vancouver, Canada). Aliquots 200 of cells were frozen in media
333 that contained 90% fetal bovine serum (HyClone, Logan, UT) and 10% dimethyl sulfoxide (Sigma-
334 Aldrich, St. Louis, MO) and stored at -70°C. Cells were stained and analyzed using a 17-color antibody
335 cocktail (Supplementary Table 1) including a PE-labeled SARS-CoV-2 S1 antibody (Supplementary
336 Table 1).

337 *Digital Droplet PCR*

338 A QIAamp Viral Mini Kit (Qiagen, Catalog #52906) was used to extract nucleic acids from 300 to 400
339 mL of plasma sample according to the manufacturer's instructions and eluted in 50 mL of AVE buffer
340 (RNase-free water with 0.04% sodium azide). The purified nucleic acids were tested immediately with a
341 Bio-Rad SARS-CoV-2 ddPCR Kit (Bio-Rad, Hercules, CA, USA). The panel was designed for
342 specifically detecting 2019-nCoV (two primer/probe sets). An additional primer/probe set was used to
343 detect the human RNase P gene in control samples and clinical specimens. RNA isolated and purified

344 from the plasma samples (5.5 mL) was added to a master mix comprising 1.1 mL of 2019-nCoV triplex
345 assay, 2.2 mL of reverse transcriptase, 5.5 mL of supermix, 1.1 mL of dithiothreitol, and 6.6 mL of
346 nuclease-free water.
347 The mixtures were then fractionated into up to 20,000 nanoliter-sized droplets in the form of a water-in-
348 oil emulsion in a QX200 Automated Droplet Generator (Bio-Rad, Hercules, CA). The 96-well real-time-
349 digital droplet polymerase chain reaction (RT-ddPCR) ready plate containing droplets was sealed with
350 foil using a plate sealer and thermocycled to reverse transcribe the RNA, before PCR amplification of
351 cDNA in a C1000 Touch thermocycler (Bio-Rad, Hercules, CA, USA). After PCR, the plate was loaded
352 into a QX200 Droplet Reader (Bio-Rad, Hercules, CA, USA) and the fluorescence intensity of each
353 droplet was measured in two channels (FAM and HEX). The fluorescence data were then analyzed with
354 QuantaSoft 1.7 and QuantaSoft Analysis Pro 1.0 Software (Bio-Rad, Hercules, CA, USA).

355

356 *Flow Cytometric Cell Sorting*

357 Cryopreserved PBMCs were quick-thawed, centrifuged, and washed in 2% BSA solution in D-
358 PBS. Cells were blocked for 5 min. in 2% BSA and then incubated at room temperature for 30
359 min. with Alexa Fluor® 488 Anti-CD45 antibody (IncellDx, 1/100 dilution), 2.5 ug of Alexa
360 Fluor® 647 Anti-CD16 antibody (BD, Cat. # 55710), and 1 ug of PerCP/Cy5.5 Anti-human
361 CD14 antibody (Biolegend, Cat. #325622). Cells were washed twice with 2% BSA/D-PBS,
362 filtered, and kept on ice for the duration of the cell sort. Data was acquired on a Sony SH800,
363 and only CD45+ cells staining positive for both CD14+ and CD16+ were sorted into test tubes
364 with 100 uL 2% BSA solution. Sort purity of control PBMCs was confirmed to be >99% by re-
365 analyzing sorted PBMCs using the same template and gating strategy.

366

367 *Single Cell Protein Identification*

368

369 Patient cells were sorted based on phenotypic markers (as above) and frozen at -80°C . Six patient
370 samples with positive flow cytometry signal and sufficient cell counts were chosen for LCMS
371 confirmation. Frozen cells were lysed with the IP Lysis/Wash Buffer from the kit according to the
372 manufacturer's protocol. 10 μg of anti-S1 mAb were used to immunoprecipitate the S1 Spike
373 protein from cell lysate of each patient. After overnight incubation with end-over-end rotation at
374 4°C and then three washes with IP Lysis/Wash Buffer, bound S1 Spike protein was eluted with the
375 elution buffer from the kit.

376 IP elution fractions were dried *in vacuo*, resuspended in 20 μL of water, pooled, and purified by
377 Agilent 1290 UPLC Infinity II on a Discovery C8 (3cm x 2.1 mm, 5 μm , Sigma-Aldrich, room
378 temperature) using mobile phase solvents of 0.1% trifluoroacetic acid (TFA) in water or
379 acetonitrile. The gradient is as follows: 5-75% acetonitrile (0.1% TFA) in 4.5 min (0.8 mL/min),
380 with an initial hold at 5% acetonitrile (0.1% TFA) for 0.5 min (0.8 mL/min). The purified protein
381 was dried *in vacuo* and resuspended in 50 μL of 100 mM HEPES, pH 8.0 (20% Acetonitrile). 1
382 μL of TCEP (100 mM) was added and the samples were incubated at 37°C for 30 min. 1 μL of
383 chloroacetamide (500 mM) was added to the samples and incubated at room temperature for 30
384 min. 1 μL rAspN (Promega 0.5 $\mu\text{g}/\mu\text{L}$) and 1 μL of LysC (Pierce, 1 $\mu\text{g}/\mu\text{L}$) were added and the
385 samples incubated at 37°C for 16 h, prior to LCMS analysis.

386

387 *LC-MS analysis*

388 Digested recombinant SARS-CoV-2 Spike S1 protein was analyzed by a high mass accuracy mass
389 spectrometer to generate a list of detectable peptides with retention time and accurate masses. An
390 Agilent 1290 Infinity II high pressure liquid chromatography (HPLC) system and an AdvanceBio

391 Peptide Mapping column (2.1 × 150 mm, 2.7 μm) were used for peptide separation prior to mass
392 analysis. The mobile phase used for peptide separation consists of a solvent A (0.1% formic acid
393 in H₂O) and a solvent B (0.1% formic acid in 90% CH₃CN). The gradient was as follows: 0–1 min,
394 3% B; 1– 30 min, to 40% B; 30–33 min, to 90% B; 33-35 min, 90% B; 37-39 min, 3% B. Eluted
395 peptides were electrosprayed using a Dual JetStream ESI source coupled with the Agilent 6550
396 iFunnel time-of-flight MS analyzer. Data was acquired using the MS method in 2 GHz (extended
397 dynamic range) mode over a mass/charge range of 50–1700 Daltons and an auto MS/MS method.
398 Acquired data were saved in both centroid and profile mode using Agilent Masshunter Workstation
399 B09 Data acquisition Software. The same analytical method was applied to immunoprecipitated
400 samples from sorted patient cells except no ms/ms was acquired.

401

402 *Viral Genome Detection by PCR and Whole Viral Genome Sequencing*

403 *Ct Determination with TaqPath Assay*

404 Five RNA samples were subjected to the TaqPath COVID-19 Combo Kit Assay (Thermo Fisher
405 Scientific Catalog no. A47814) to assess the cycle of threshold. TaqPath COVID-19 Combo Kit assay
406 was performed according to recommendations of the EUA, using the Applied BioSystems QuantStudio 7
407 Flex (Thermo Fisher Scientific Catalog no. 4485701).

408 *Whole Genome Sequencing of Samples with Ion AmpliSeq*

409 Five RNA samples were subjected to AmpliSeq library preparation using the Ion AmpliSeq Library Kit
410 2.0 (Thermo Fisher Scientific Catalog no. 4480441) and the Thermo Fisher Scientific Insight panel,
411 which consists of 238 amplicons in a two pool design against SARS-CoV-2 and seven amplicons as
412 human controls. Libraries were prepared following manufacturer's recommendations. Final libraries were
413 amplified using 5 cycles of amplification and libraries were cleaned up using 0.5X right sided cleanup

414 and 1.2X left sided cleanup using Kapa Pure Beads (Roche Catalog no 17983298001). Final libraries were
415 quantified using Ion Library TaqMan Quantitation Kit (ThermoFisher Catalog no. 4468802). Samples
416 were pooled in an equimolar distribution and loaded on to the Ion Chef Instrument (ThermoFisher
417 Catalog no. 4484177) for Templating onto a 510 chip. The prepared chip was then loaded onto a
418 GeneStudio S5 Prime (ThermoFisher Catalog no. A38196) for sequencing.

419 ***Genome Assembly, Quality Control, and Sequencing Analysis***

420 Sequencing reads were aligned to the SARS-CoV-2 genome (build NC_045512.2) and human
421 transcriptome (build GRCh37) using the Thermo Fisher Scientific TMAP aligner. Default parameters
422 were used except for the *--context* flag.

423 Coverage analysis was performed by the coverageAnalysis plugin in Thermo Fisher Scientific Torrent
424 Suite software. Reads in the human controls were evaluated for quality control. Per-base coverage,
425 average coverage, and percent genome covered at various depth thresholds were assessed using custom
426 software. Read length distribution versus read quality (MAPQ score) were further evaluated.

427 Variant calling was performed on SARS-CoV-2 using the variantCaller plugin. Callable regions were
428 identified as regions with read depth ≥ 20 after filtering reads with $\text{MAPQ} < 10$. Variants were filtered
429 for quality by removing mutations with allele frequency (AF) < 0.5 in the callable regions. Lineage
430 determination was made with pangoleARN v1.2.13 using filtered-in mutations.

431

432

433

434

435

436

437

438 **REFERENCES**

439

- 440 1. R. Rubin. As Their Numbers Grow, COVID-19 “Long Haulers” Stump
441 Experts. *JAMA*. **324**, 1381–1383 (2020). doi:10.1001/jama.2020.17709
- 442 2. <https://www.cdc.gov/coronavirus/2019-ncov/hcp/clinical-care/post-covid-conditions.html>
443 (April 8, 2021).
- 444 3. X.H. Yao, Z.C. He, T.Y. Li, H. R. Zhang, Y. Wang, H. Mou, Q. Guo, S.C. Yu, Y. Ding,
445 X. Liu, Y.F. Ping, X.W. Bian. Pathological evidence for residual SARS-CoV-2 in
446 pulmonary tissues of a ready-for-discharge patient. *Cell Res*. **30**, 541-543 (2020). doi:
447 10.1038/s41422-020-0318-5. Epub 2020 Apr 28. PMID: 32346074; PMCID:
448 PMC7186763.
- 449 4. R. Nienhold, Y. Ciani, V.H. Koelzer, A. Tzankov, J.D. Haslbauer, T. Menter, N. Schwab,
450 M. Henkel, A. Frank, V. Zsikla, N. Willi, W. Kempf, T. Hoyler, M. Barbareschi, H.
451 Moch, M. Tolnay, G. Cathomas, F. Demichelis, T. Junt, K.D. Mertz. Two distinct
452 immunopathological profiles in autopsy lungs of COVID-19. *Nat Commun*. **11**, 5086
453 (2020). doi: 10.1038/s41467-020-18854-2.
- 454 5. B.K. Patterson, J. Guevarra-Coto, R. Yogendra, E. B. Francisco, E. Long, A. Pise, H.
455 Rodrigues, P. Parikh, J. Mora. R.A. Mora-Rodríguez. Immune-based prediction of
456 COVID-19 severity and chronicity decoded using machine learning. *Front Immunol*
457 (2021) <https://doi.org/10.3389/fimmu.2021.700782>.
- 458 6. T.S. Kapellos, L. Bonaguro, I. Gemünd, N. Reusch, A. Saglam, E. R Hinkley, J. L.
459 Schultze. Human monocyte subsets and phenotypes in major chronic inflammatory
460 diseases. *Front Immunol* **10**, 1–13 (2020) <https://doi.org/10.3389/fimmu.2019.02035>.
- 461 7. L. Ziegler-Heitbrock. The CD14+ CD16+ blood monocytes: their role in infection and
462 inflammation. *J Leuk Biol* **81**, 584–592 (2007). <https://doi.org/10.1189/jlb.0806510>.
- 463 8. M. Rutkowska-Zapała, M. Suski, R. Szatanek, M. Lenart, K. Węglarczyk, R. Olszanecki,
464 T. Grodzicki, M. Strach, J. Gąsowski, M. Siedlar. Human monocyte subsets exhibit
465 divergent angiotensin I-converting activity *Clin Exp Immunol* **181**, 126–132 (2015).
- 466 9. R. Mukherjee, P. Kanti Barman, P. Kumar Thatoi, R. Tripathy, B. Kumar Das, B.
467 Ravindran. Non-Classical monocytes display inflammatory features: Validation in Sepsis
468 and Systemic Lupus Erythematosus. *Sci Rep*. **5**, 13886 (2015). doi: 10.1038/srep13886.
- 469 10. D. Michlmayr, P. Andrade, K. Gonzalez, A. Balmaseda, E. Harris. CD14+CD16+
470 monocytes are the main target of Zika virus infection in peripheral blood mononuclear
471 cells in a paediatric study in Nicaragua. *Nature Microbiology*, **2**, 1462–1470 (2017).
472 <https://doi.org/10.1038/s41564-017-0035-0>
- 473 11. Coquillard G, Patterson BK. Determination of hepatitis C virus-infected, monocyte
474 lineage reservoirs in individuals with or without HIV coinfection. *J Infect Dis*. **200**, 947-
475 954 (2009). doi: 10.1086/605476. PMID: 19678757.
- 476 12. P. Ancuta, K.J.Kunstman, P. Autissier, T. Zaman, D. Stone, S.M. Wolinsky, D.Gabuzda.
477 CD16+ monocytes exposed to HIV promote highly efficient viral replication upon
478 differentiation into macrophages and interaction with T cells. *Virology* **344**, 267–276
479 (2006). <https://doi.org/10.1016/j.virol.2005.10.027>
- 480 13. A.A. Patel, Y. Zhang, J.N.Fullerton, L. Boelen,, A. Rongvaux, A.A. Maini, V.Bigley,
481 R.A. Flavell, D.W. Gilroy, B. Asquith, D. Macallan, S. Yona. The fate and lifespan of

- 482 human monocyte subsets in steady state and systemic inflammation. *J Exp Med.* **214**,
483 1913-1923 (2017). doi: 10.1084/jem.20170355. Epub 2017 Jun 12. PMID: 28606987;
484 PMCID: PMC5502436.
- 485 14. P. Ancuta, K.Y. Liu KY, V. Misra, V.S. Wacliche, A. Gosselin, X. Zhou, D. Gabuzda.
486 Transcriptional profiling reveals developmental relationship and distinct biological
487 functions of CD16+ and CD16- monocyte subsets. *BMC Genomics* **10**, 403 (2009). doi:
488 10.1186/1471-2164-10-403. PMID: 19712453; PMCID: PMC2741492.
- 489 15. T. Tak, R. van Groenendael, P. Pickkers, L. Koenderman. Monocyte subsets are
490 differentially lost from the circulation during acute inflammation induced by human
491 experimental endotoxemia. *J Innate Immun.* **9**, 464-474 (2017). doi: 10.1159/000475665.
492 Epub 2017 Jun 23. PMID: 28641299; PMCID: PMC6738874.
- 493 16. C. Auffray, D. Fogg, M. Garfa, G. Elain, O. Join-Lambert, S. Kayal, S. Sarnacki, A.
494 Cumano, G. Lauvau, F. Geissmann. Monitoring of blood vessels and tissues by a
495 population of monocytes with patrolling behavior. *Science* **317**, 666-670 (2007). doi:
496 10.1126/science.1142883. PMID: 17673663.
- 497 17. S.T. Gren, T.B. Rasmussen, S. Janciauskiene. A single-cell gene-expression profile
498 reveals inter-cellular heterogeneity within human monocyte subsets. *PLoS One* **10**,
499 e0144351 (2015). doi: 10.1371/journal.pone.0144351. PMID: 26650546; PMCID:
500 PMC4674153.
- 501 18. K.L. Wong, J.J. Tai, W.C. Wong, H. Han, X. Sem, W.H. Yeap, P. Kourilsky, S.C. Wong.
502 Gene expression profiling reveals the defining features of the classical, intermediate, and
503 nonclassical human monocyte subsets. *Blood.* **118**, e16-31 (2011). doi: 10.1182/blood-
504 2010-12-326355. Epub 2011 Jun 7. PMID: 21653326.
- 505 19. A. Jafarzadeh, P. Chauhan, B. Saha, S. Jafarzadeh, M. Nemati. Contribution of
506 monocytes and macrophages to the local tissue inflammation and cytokine storm in
507 COVID-19: Lessons from SARS and MERS, and potential therapeutic interventions. *Life*
508 *Sci.* **257**, 118102 (2020). doi: 10.1016/j.lfs.2020.118102. Epub 2020 Jul 18. PMID:
509 32687918; PMCID: PMC7367812.
- 510 20. Y. Zhou, B. Fu, X. Zheng. Pathogenic T-cells and inflammatory monocytes incite
511 inflammatory storms in severe COVID-19 patients, *National Science Review* **7**, 998–1002
512 (2020).
- 513 21. C.E. Olingy, C.L. San Emeterio, M.E. Ogle, J.R. Krieger, A.C. Bruce, D.D. Pfau, B.T.
514 Jordan, S.M. Peirce, E.A. Botchwey. Non-classical monocytes are biased progenitors of
515 wound healing macrophages during soft tissue injury. *Sci Rep.* **7**, 447 (2017). doi:
516 10.1038/s41598-017-00477-1. PMID: 28348370; PMCID: PMC5428475.
- 517 22. P.B. Narasimhan, P. Marcovecchio, A.A.J. Anouk, C.C. Hedrick. Nonclassical
518 monocytes in health and disease. *Ann Rev Immunol* **37**, 439-456 (2019).
- 519 23. V. Vila-del Sol, C. Punzón, M. Fresno. IFN-gamma-induced TNF-alpha expression is
520 regulated by interferon regulatory factors 1 and 8 in mouse macrophages. *J Immunol*
521 **181**:4461-4470 (2008). doi: 10.4049/jimmunol.181.7.4461. PMID: 18802049.
- 522 24. T. Matsumiya, K. Ota, T. Imaizumi, H. Yoshida, H. Kimura, K. Satoh. Characterization
523 of Synergistic Induction of CX3CL1/Fractalkine by TNF- α and IFN- γ in vascular
524 endothelial cells: an essential role for TNF- α in post-transcriptional regulation of
525 CX3CL1. *J Immunol* **184**, 4205-4214 (2010). DOI: 10.4049/jimmunol.0903212.
- 526 25. S.M. Ong, E. Hadadi, T.M. Dang, W.H. Yeap, C.T. Tan, T.P. Ng, A. Larbi,
527 S.C. Wong. The pro-inflammatory phenotype of the human non-classical monocyte subset

- 528 is attributed to senescence. *Cell Death Dis* **9**, 266 (2008).
529 <https://doi.org/10.1038/s41419-018-0327-1>.
530 26. C.F. Pereira, J. Middel, G. Jansen, H.S. Nottet. Enhanced expression of fractalkine in
531 HIV-1 associated dementia. *J Neuroimmunol* **115**, 168-115 (2001). doi: 10.1016/s0165-
532 5728(01)00262-4. PMID: 11282167.
533 27. A.R. Jajtner, J.R. Townsend, K.S. Beyer, A.N. Varanoske, D.D. Church, L.P. Oliveira,
534 K.A. Herrlinger, S. Radom-Aizik, D.H. Fukuda, J.R. Stout, J.R. Hoffman. Resistance
535 exercise selectively mobilizes monocyte subsets: role of polyphenols. *Med Sci Sports*
536 *Exerc.* **50**, 2231-2241 (2018). doi: 10.1249/MSS.0000000000001703. PMID: 29957728.

537
538

539 **Ethics**

540 Informed consent was obtained from all participants.

541

542 **Data and materials availability:**

543 All requests for materials and raw data should be addressed to the corresponding author

544

545 **Competing interests:**

546 B.K.P, A.P., H.R., E.L, and EBF. are employees of IncellDx, Inc

547 TJT, PS, SH, DM are employees of Avrok Laboratories, Inc

548

549 **Author contributions:**

550 R.Y. and P.P. organized the clinical study and actively recruited patients.

551 B.K.P, A.P., H.R., X.E, E.L., J.B.S., TJT, PS, SH, DM performed experiments and analyzed the data.

552 J.G-C., R.A.M., J.M., X.C. performed the statistics and bioinformatics

553 B.K.P., J.M., EBF, J.G-C., R.A.M. wrote the draft of the manuscript and all authors contributed to

554 revising the manuscript prior to submission.

555

556 **Funding:** None

557

558

559

560

561

562

563

564

565

566

567

568

569

570

571

572

573

574

575 **TABLE and FIGURE LEGENDS**

576

577 Table 1. Molecular analysis of study participants.

COVID-19 Status	Sars-CoV-2 RNA+		Months Post-Infection
	NS	PBMCs	
HC 1	-	-	n/a
HC 2	-	-	n/a
HC 3	-	-	n/a
HC 4	-	-	n/a
HC 5	-	-	n/a
HC 6	-	-	n/a
HC 7	-	-	n/a
HC 8	-	-	n/a
Asymptomatic	+	+	n/a
Severe 1	+	-	n/a
Severe 2	+	+	n/a
Severe 3	+	-	n/a
Severe 4	+	-	n/a
Severe 5	+	-	n/a
Severe 6	+	-	n/a
Severe 7	+	+	n/a
Severe 8	+	-	n/a
Severe 9	+	-	n/a
Severe 10	+	+	n/a
Severe 11	+	+	n/a
LH 1	+	-	13
LH 2	+	-	14
LH 3	+	-	6
LH 4	+	-	11
LH 5	+	+	15
LH 6	+	-	13
LH 7	+	-	12
LH 8	+	-	7
LH 9	+	-	14
LH 10	+	-	13
LH 11	+	-	12
LH 12	+	-	12
LH 13	+	-	6
LH 14	+	-	14
LH 15	+	-	13
LH 16	+	-	9
LH 17	+	-	11
LH 18	+	-	7

LH 19	+	-	14
LH 20	+	-	11
LH 21	+	-	13
LH 22	+	-	10
LH 23	+	-	8
LH 24	+	-	7
LH 25	+	-	12
LH 26	+	-	15

578 **Table 2: Average Coverage and Percent Bases Covered at 20x** While the percent of bases
579 covered varied across patients, all were less than 20% at 10X, and less at 20X coverage. In no
580 case was full length viral genome RNA detected, consistent with a lack of replication competent
581 viral infection.

582

Sample	Average Coverage	Percent Bases Covered at 10x	Percent Bases Covered at 20x
02-03_20210625	171.64	19.18	15.24
ABA-2_20210625	59.67	14.04	10.42
BGI-2_20210625	24.17	10.81	7.69
CST-2_20210625	40.29	11.71	7.79
RG_20210625	592.87	12.6743	10.16

583

584

585

586

587

588

589

590

591

592

593

594

595

596

597

598

599

600

601

602

603

604

605 **Figure 1.** Quantification of classical, intermediate and non-classical monocytes in PASC (LH).
606 Non-classical monocytes were significantly elevated in severe COVID-19 and in PASC.

607
608 **Figure 2.** High parameter flow cytometric quantification of SARS-CoV-2 S1 protein in
609 monocytic subsets. Cells were gated on CD45 then analyzed for CD14 and CD16 expression.
610 Classical monocytes are green, intermediate monocytes are red and non-classical monocytes are
611 blue.

612
613 **Figure 3.** Quantification of SARS-CoV-2 S1 protein in monocyte subsets isolated from healthy
614 controls (HC), severe COVID-19 (severe), and PASC patients (LH). SARS-CoV-2 S1 protein
615 was expressed in non-classical monocytes in both severe and PASC individuals. The amount of
616 expression was statistically significant.

617
618 **Figure 4.** LCMS confirmation of the presence of S1 subunit in samples LH1-6. A. Extracted ion
619 chromatogram (EIC) displaying the NLREFVFK peptide. The retention time matches that of the
620 NLREFVFK peptide in the commercial S1 standard. B. Mass Spectra of the NLREFVFK from
621 both the commercial standard and patient LH1. The Spectra show the same mass and isotope
622 distribution.

623 **Figure 5:** High Quality Mutations in the Callable Regions. Only fragmented viral RNA was
624 identified in the five patients, but multiple mutations throughout the viral genome were
625 identified, the vast majority of which were unique to each patient. Overall coverage was less than
626 20%, and no complete sequence in any portion of the viral genome was detected, including in the
627 spike gene encoding the S1 subunit identified by protein analysis in these patients.

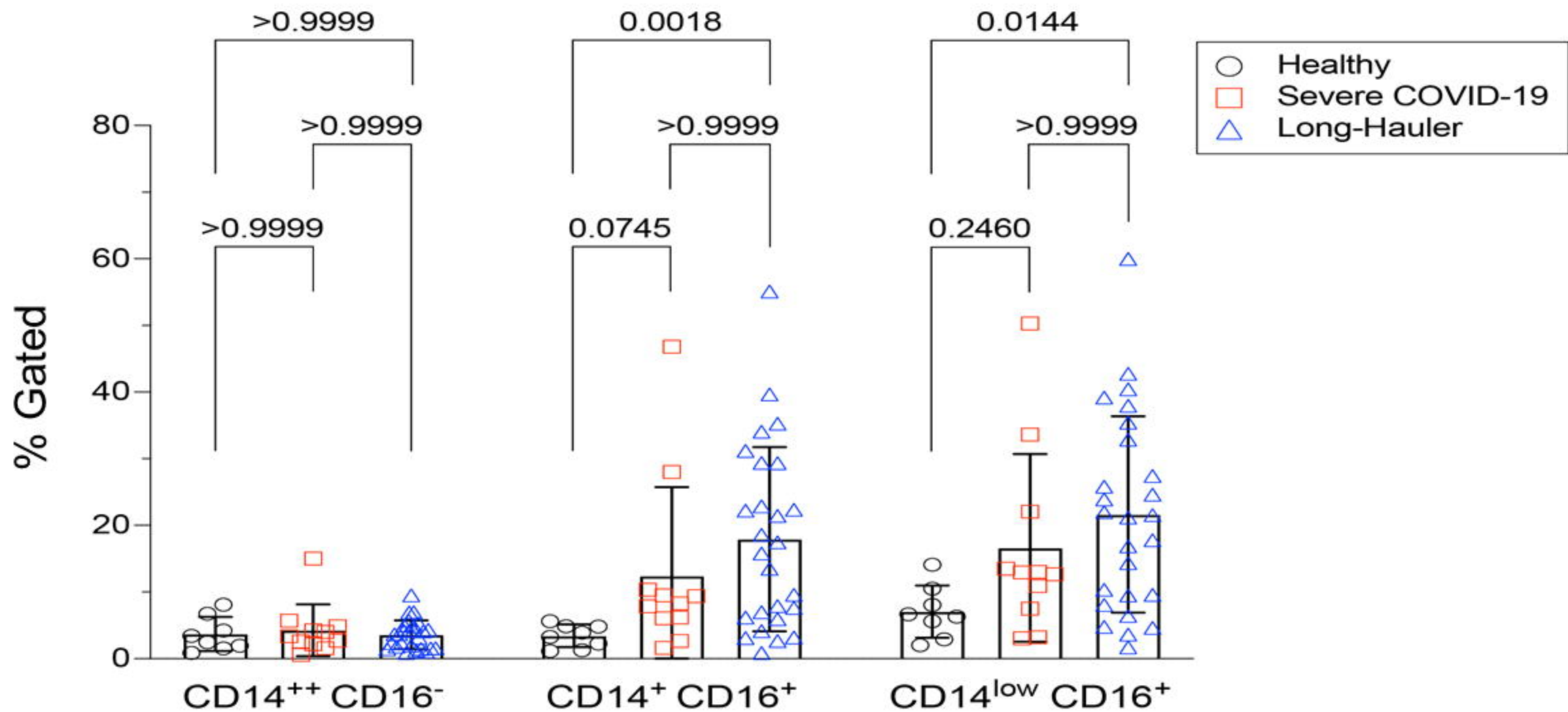
628

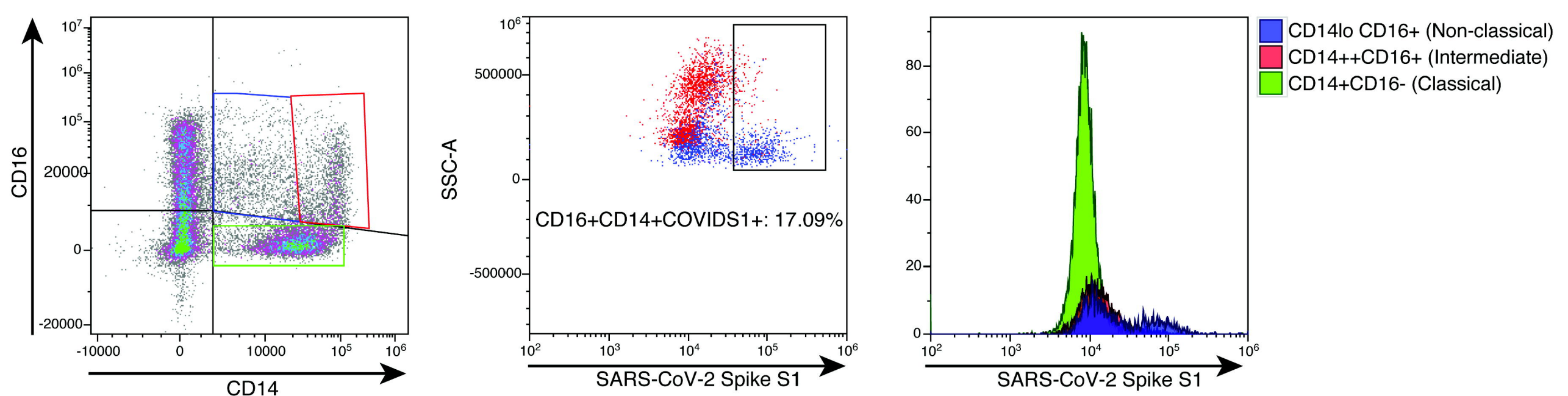
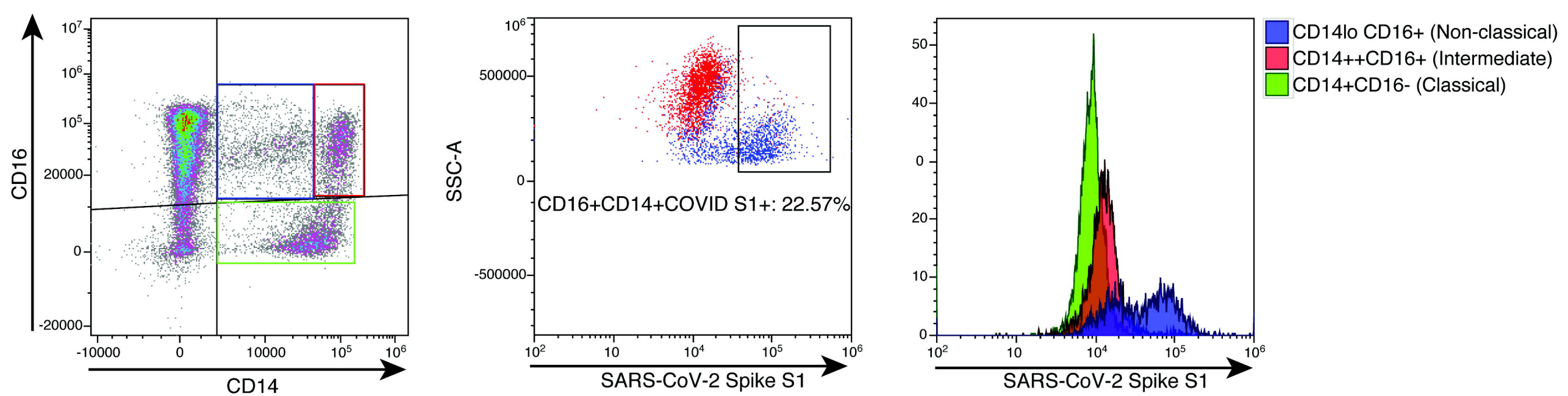
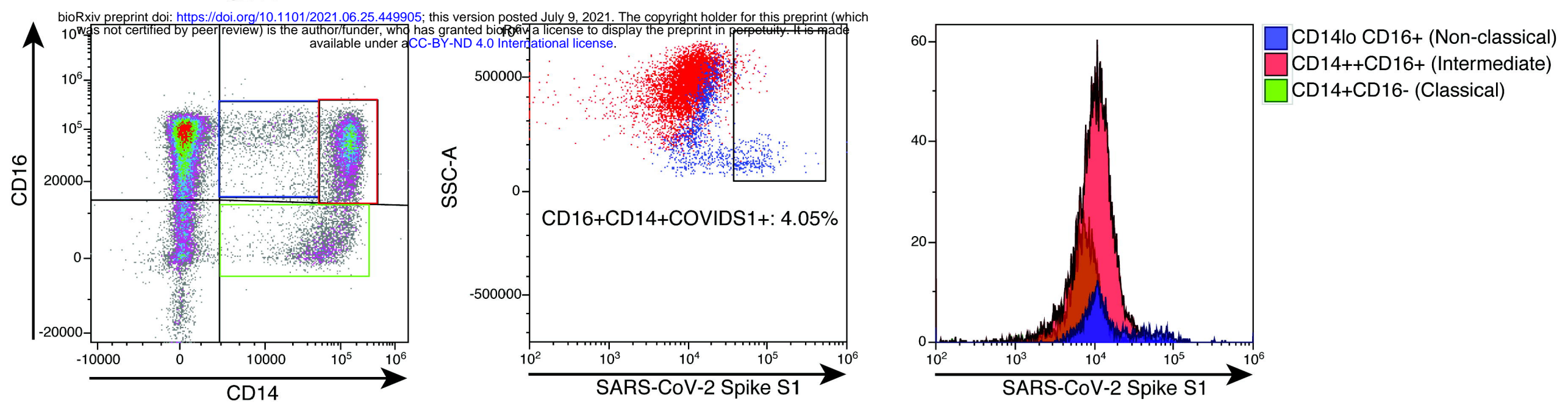
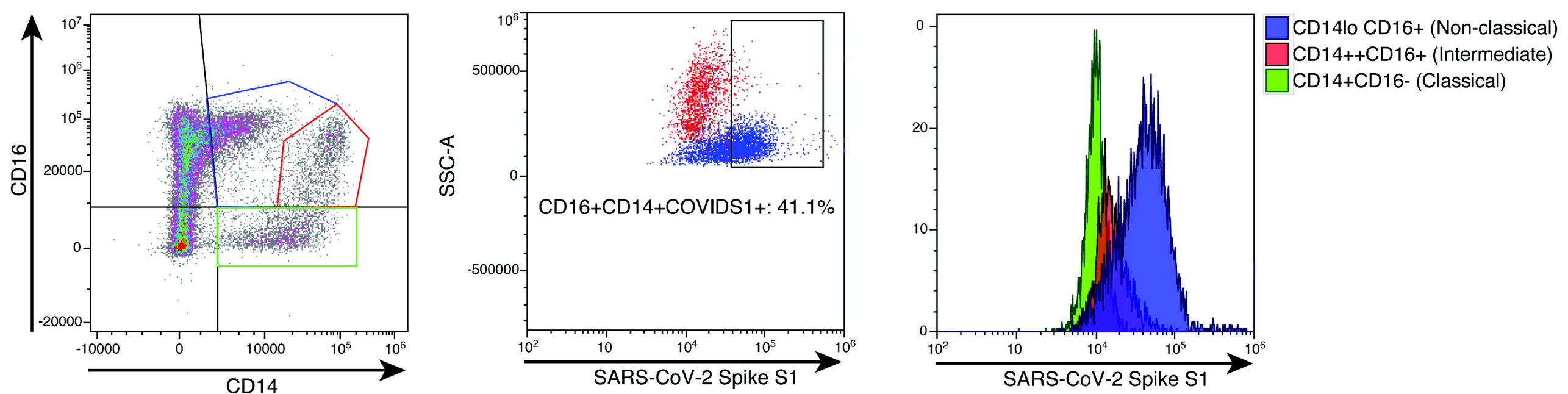
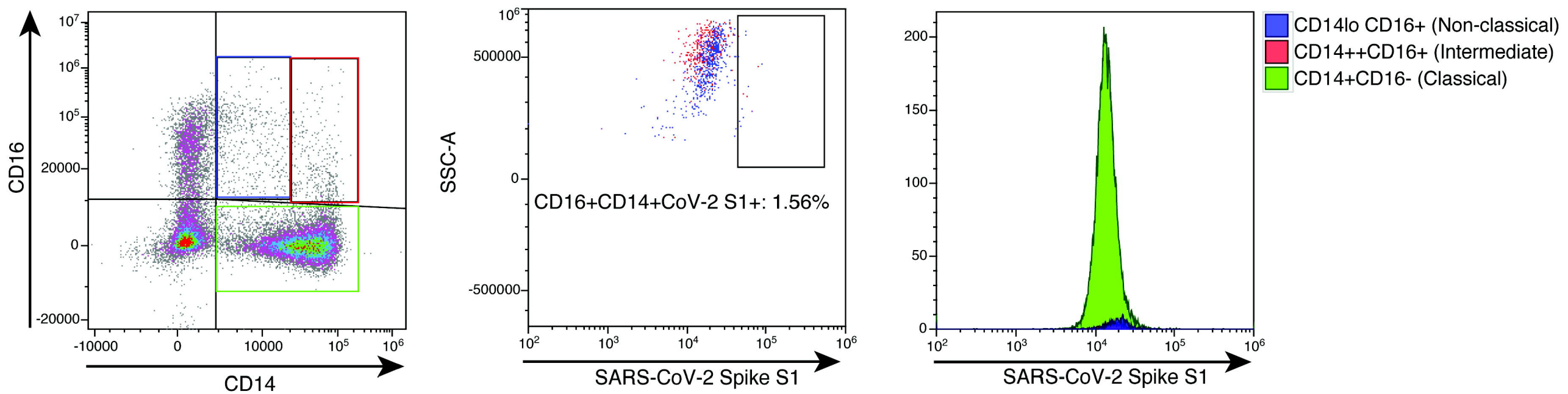
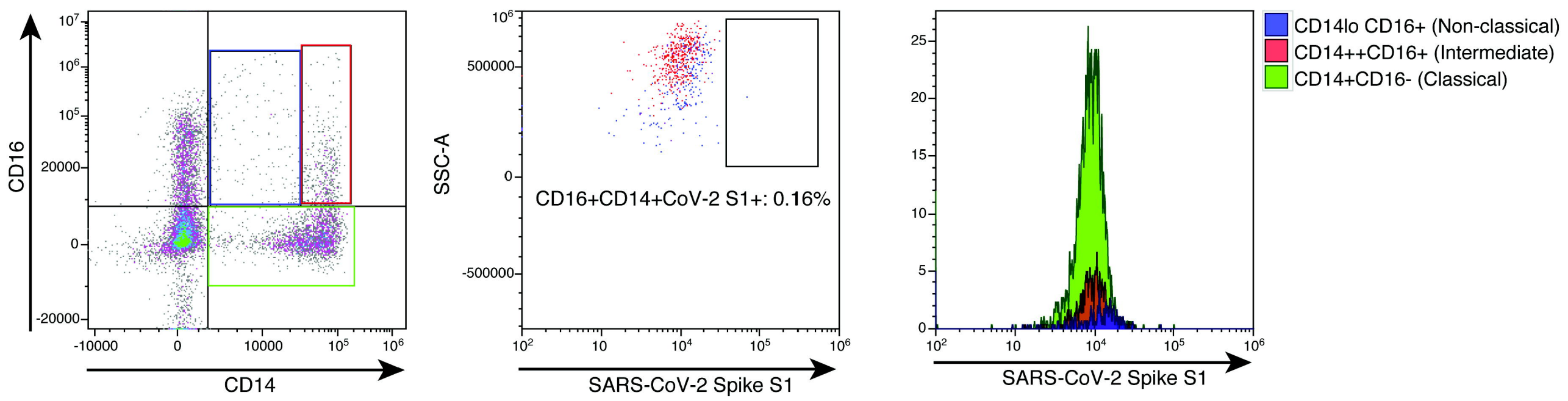
629

630

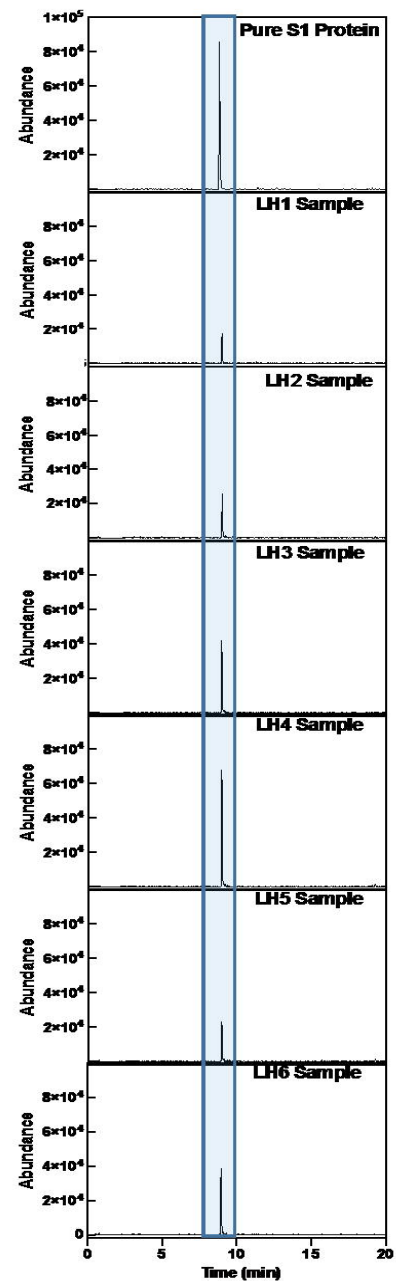
631

632





A



B

